Optimization of hyperplanar transition states

Gísli H. Jóhannesson and Hannes Jónsson
Department of Chemistry 351700, University of Washington, Seattle, Washington 98195-1700 and Faculty of Science, VR-II, University of Iceland, 107 Reykjavík, Iceland

(Received 25 September 2000; accepted 13 September 2001)

A method for systematically finding the optimal orientation and location of a hyperplanar dividing surface during a transition state theory calculation of a transition rate is presented. The optimization can be carried out during a reversible work evaluation of the free energy barrier. An application to Al adatom diffusion on an Al(100) surface is described. There, the method can converge to give the free energy barrier for the optimal mechanism, a concerted displacement, even when the calculation is initially set up for the less optimal hop mechanism. This illustrates that the method can reveal the optimal mechanism of a transition even when the calculation is started with an incorrect guess.
 [DOI: 10.1063/1.1415499]

I. INTRODUCTION

Transition state theory (TST) (Refs. 1, 2) is a highly successful, approximate theory for calculating rates of transitions in atomic systems where the classical equations of motion can be used to describe the dynamics of the atoms. The basic idea is to divide the configuration space of the system by a dividing surface into a region corresponding to an initial state and a region corresponding to a final state. If the system has D dimensions, the dividing surface has $D-1$ dimensions. The rate of the transition is then approximated as the probability of finding the system in the dividing surface times the rate of escape from the dividing surface towards the final state. Often, the TST estimate of the rate is accurate enough, but it is important to choose the dividing surface well. A poorly chosen dividing surface leads to a poor rate estimate. The choice of a dividing surface can be nontrivial even for simple systems. A major challenge is to find good dividing surfaces in high-dimensional systems. When a more precise estimate of the rate is needed, the correction to TST can be obtained from classical dynamics simulations where the system is started in the dividing surface and the recrossings of the classical trajectory through the dividing surface monitored. This is a simple calculation if the TST estimate is not off by more than one or two orders of magnitude, again requiring that the transition state dividing surface be chosen well. In the end, TST provides a procedure for dealing with the time scale problem in atomic scale transitions in condensed phases, namely, the very long time scale for reactive events compared with the fast time scale of atomic vibrations.

TST is most often applied within the harmonic approximation, where the partition function of the system in the dividing surface and in the initial state is approximated by a harmonic partition function.[3] The problem then reduces to finding all the relevant saddle points on the potential energy surface. The assumption here is that only a few saddle points are needed. At each saddle point, the dividing surface is taken to be the hyperplane going through the saddle point with the normal given by the displacement vector of the unstable mode. For many systems the harmonic approximation is, however, not accurate enough. This is likely to be the case when the atoms are weakly bound compared with the thermal energy and when the transition involves a region on the potential energy surface with many saddle points.

The choice of the dividing surface can be guided by a variational principle. It can be shown that TST always overestimates the rate, so the optimal dividing surface is the one that leads to the smallest estimate of the rate.[1,4] Truhlar and co-workers have formulated many different versions of variational TST, where the full calculation of the rate constant is repeated for different choices of the transition state.[5] Since any recrossing of the dividing surface leads to an overestimate in the rate constant, one might assume that minimizing the number of recrossings will give the lowest rate estimate. Makarov and Metiu have showed that this may not be the case.[6] A more rigorous formulation is in terms of the free energy. As was pointed out by Chandler, the dividing surface with the highest free energy gives the best TST rate estimate.[7]

The free energy of the dividing surface can be evaluated by calculating the reversible work (RW-TST) of pushing the system from the initial state towards the final state. The dividing surface of maximum free energy is the optimal choice for the transition state, since it gives the smallest rate estimate. A general formulation, including arbitrary shape of the dividing surface, has been developed by Ciccotti and co-workers.[8] When the dividing surface is taken to be a hyperplane, the equations for evaluating the reversible work simplify greatly. Mills, Schenter, and Jónsson showed that the free energy consists of a contribution from the translation of the hyperplane against the force acting on it and a contribution from the rotation of the hyperplane against the generalized torque.[9] An equivalent formulation was later given by Neria, Fischer, and Karplus.[10]

Previously, the orientation of the hyperplane (or the shape of the dividing surface in the more general formulation of Ciccotti and co-workers) has been a predetermined function of the location. Often the distance between some chosen atoms, or the minimum energy path for the transition is used

to parametrize the progression of the hyperplane from the initial state towards products in the reversible work calculation. The orientation of the hyperplane is then predetermined, for example with the normal vector parallel to the tangent of the minimum energy path.[9]

We present here a new method where the orientation of the hyperplane is not a predetermined function of the reaction coordinate, but is optimized at each step of the reversible work calculation. The free energy of the hyperplane is maximized with respect to both translation and orientation. This can lead to significantly better transition state dividing surfaces and thereby better estimates of the rate. An optimization with respect to just the reaction coordinate is a one-dimensional optimization. The orientational optimization is D-2 dimensional and represents a much larger degree of optimization. As a result, the inclusion of orientational optimization makes it less critical which path is chosen to parametrize the hyperplane progression to begin with. We have here used a straight line interpolation between initial and final states. As will be demonstrated below, the large flexibility and systematic optimization of the hyperplanar dividing surface in this new method can lead to convergence to a transition state for a different optimal transition mechanism than the one assumed initially, thereby correcting an incorrect preconceived notion of the transition mechanism. The method is easy to implement and requires only the energy of the system and the force acting on the atoms.

Ultimately, a robust method that does not require knowledge of the final state and the transition mechanism could be used to calculate the long time scale evolution of a system. This type of approach has been formulated for harmonic systems.[11] The method presented here could, in favorable cases, be used to simulate long time scale dynamics in the more general, anharmonic cases. The use of hyperplanar dividing surfaces in the current formulation, however, restricts the applicability of the method, as will be discussed below.

II. METHODOLOGY

TST is based on three assumptions.[1] The first one is the Born–Oppenheimer (adiabatic) approximation. The movement of the nuclei in the system is assumed to be slow enough that the electrons are always in the lowest quantum state for any given configuration of the nuclei. The transition must not involve electronic excitations. We will focus here entirely on classical systems, i.e., systems where the motion of the nuclei of the atoms can be described by classical mechanics. Extensions of TST to quantum systems have been presented and the methodology for optimizing the dividing surface could be generalized to quantum transition states within that formulation.[12]

The second assumption introduces a hypersurface in the configuration space of the nuclei, separating the reactant and product regions, such that if a path crosses this surface going from one of the states to the other, it will not recross the surface for a long time.

The third assumption is that thermal equilibrium has been reached within the reactant region of configuration space and the transition rate is low enough that an equilibrium distribution of energy is maintained in all degrees of freedom of the reactants.

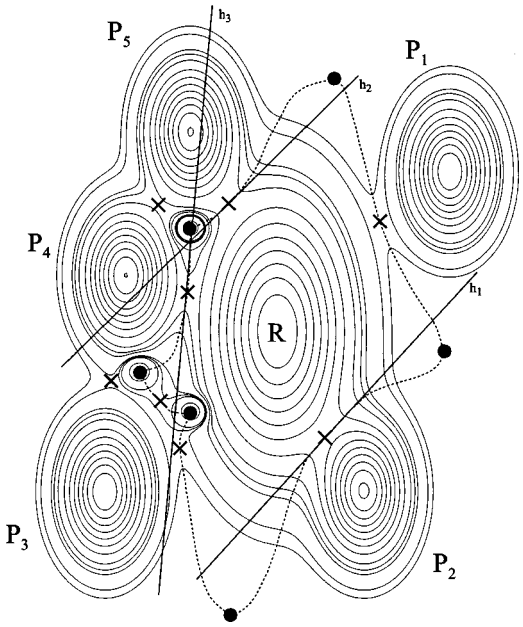

FIG. 1. A two-dimensional model system illustrating the use of hyperplanes as dividing surfaces. The reacting region R is surrounded by five product regions P_1-P_5. First order ($\times$) and second order ($\bullet$) saddle points are shown. The optimal TST dividing surface in the absence of entropic effects follows the potential energy ridge as indicated by the dashed curve. Three hyperplanar tangent surfaces are shown, h_1-h_3. Near the saddle points, these can be good approximations to the optimal dividing surface. However, if second order saddle points are low in energy and/or the potential energy ridge is highly curved near the first order saddle points, the hyperplane may not prevent the system from slipping into an adjacent product well (for example into state P_4 when confined to hyperplane h_2).

If any classical trajectory originating in the reactant region recrosses the dividing surface any number of times, TST will give an overestimate for the exact rate constant, $k^{\mathrm{TST}} \geqslant k^{\mathrm{EXACT}}$.[1,4] If there exists a dividing surface with no recrossings, then the TST rate constant will be exact. The transition state theory rate constant, k^{TST}, is given by

$$k^{\mathrm{TST}} = \frac{\langle |v_\perp| \rangle}{2} \frac{Q^\ddagger}{Q^R}, \tag{1}$$

where $\langle |v_\perp| \rangle /2$ is the average velocity normal to the dividing surface in the direction of the products, $Q^\ddagger$ is the configuration integral of the system confined to the dividing surface, Q^R is the configuration integral of the system in the reactant region.

If multiple products can be formed, then the transition state can be chosen as a dividing surface surrounding the reactant state region and the TST rate constant is then the total rate of escape. Figure 1 shows a reactant region R surrounded by five product regions P_1-P_5. An optimal dividing surface, in the absence of entropic effects follows the potential energy ridge and is a curved surface. In general it is difficult to construct such a surface. A simple approximation is to use the tangent hyperplanes going through the saddle points to represent the dividing surface locally. For example, hyperplane h_1 in Fig. 1 is a good approximation to the dividing surface for the transition from R to P_2. If the poten-

tial energy rises quickly away from the saddle point, the system will be trapped in the bottleneck region when confined to h_1. However, if another product region is near the saddle point and the potential energy does not rise significantly in between the two, or if the potential energy ridge is highly curved, then the hyperplane constraint will not confine the system to the bottleneck region. This is illustrated with hyperplane h_2 in Fig. 1 for the transition from R to P_5. For a high enough temperature, h_2 will not give a good approximation to the dividing surface between R and P_5.

A. Fixed hyperplane orientation

A reversible work formulation of TST including curved reaction coordinates was developed by Mills and co-workers.[9] A configuration integral of the system confined to a hyperplane in the reactant region, Q^{Z^R}, is introduced,

$$k^{\mathrm{RWTST}}=\frac{\langle|v_\perp|\rangle}{2}\frac{Q^{Z^R}}{Q^R}\frac{Q^\ddagger}{Q^{Z^R}}. \tag{2}$$

The last ratio of configuration integrals in this equation can be written in terms of a free energy, $e^{-\Delta A/k_BT}$, where k_B is the Boltzmann constant and T is the temperature. Here, ΔA is the free energy difference between two hyperplanes, one located near the reactant state and the other one at the dividing surface. The rate constant then becomes

$$k^{\mathrm{RWTST}}=\frac{\langle|v_\perp|\rangle}{2}\frac{Q^{Z^R}}{Q^R}e^{-\Delta A/k_BT}. \tag{3}$$

The free energy difference is calculated by evaluating the reversible work required to translate and rotate the hyperplane from Z^R to the dividing surface. For each position of the plane, a thermal average of the force acting on the system is calculated. This is illustrated in Fig. 2. The evaluation of the prefactor $(\langle|v_\perp|\rangle/2)(Q^{Z^R}/Q^R)$ is discussed in detail in Secs. II F and II G.

In order to describe the progression of the hyperplane, a path connecting the reactants and products is specified and the distance from a reference point in the reactant region, **R**, to the point of intersection between the path and the hyperplane, becomes a progress variable, s, scaled such that $s=0$ at **R** and $s=1$ at **P**. Often, the minimum energy path (MEP) is chosen.[9] The MEP is a natural choice for a reaction coordinate when the transition is dominated by a single trough in the potential energy surface and when entropic effects are not so strong that the free energy landscape becomes significantly different from the potential energy landscape. The MEP can be found efficiently using the nudged elastic band method.[13–15] In previous calculations the orientation of the hyperplane was a predetermined function of s. The normal of the hyperplane, $\hat{\mathbf{n}}_s$, was taken to be the tangent to the MEP at s. This ensures that the orientation of the hyperplane near the saddle point is such that the normal is in the direction of the unstable mode of the potential surface.

The free energy change between an initial hyperplane and a plane further along the path is given by the line integral,

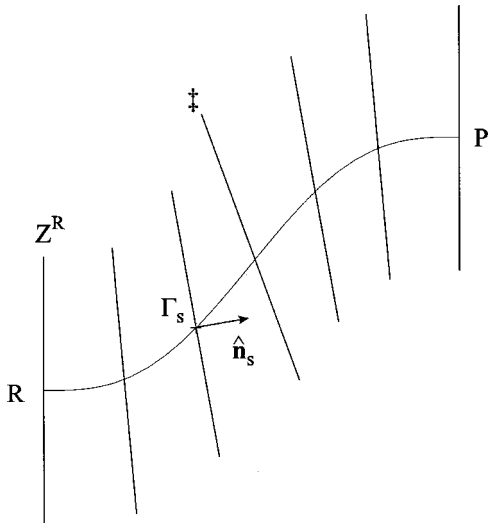

FIG. 2. A path connecting the reactant, R, and product, P, is used to parametrize the progression of the hyperplane during reversible work evaluation of the free energy barrier. In the OH-TST method the orientation of the hyperplane as well as the location of the hyperplane is systematically adjusted to find the maximum free energy barrier. This gives the optimal hyperplanar transition state. The hyperplane is characterized by the normal, $\hat{\mathbf{n}}_s$, and the intersection with the path, $\mathbf{\Gamma}_s$, where s is a scalar that runs from 0 in the reactant state to 1 in the product state.

$$\Delta A(s)=-\int_0^s\langle F_n(1-\kappa R_t)\rangle_{s'}ds', \tag{4}$$

where $F_n=F(\mathbf{r}_s)\cdot\hat{\mathbf{n}}_s$ is the normal component of the force acting on the system in the plane at configuration $\mathbf{r}_s$, $R_t=(\mathbf{r}_s-\mathbf{\Gamma}_s)\cdot d\mathbf{n}_s/d\theta$, and $\kappa=d\theta/ds$ is the first order curvature of the path.[9]

With the extension of the method, presented below, there is no need to use the minimum energy path. A straight line interpolation between **R** and **P** has been used in the applications presented here.

B. Introduction of orientational optimization

Here, we present an extension of the reversible work formulation where optimization of the hyperplane orientation is incorporated into the reversible work calculation. With little additional computation, the evaluation of the free energy barrier then naturally leads to an optimal hyperplanar dividing surface. We will refer to this method as optimal hyperplanar TST (OH-TST). The method involves rotating as well as translating the hyperplanar dividing surface during the reversible work calculation. The hyperplane is moved against the translational force acting on it and is rotated against the rotational force acting on it until both forces are sufficiently small. Since the reversible work of moving and rotating the plane represents an increase in the free energy, the optimized hyperplanar surface corresponds to a maximum in the free energy.

Let **r** represent the configuration of a system in an N-dimensional configuration space. The potential energy is given by the function $V(\mathbf{r})$. The force acting on the system is given by $\mathbf{F}(\mathbf{r})=-\nabla V(\mathbf{r})$. The initial and final states, **R** and **P**, are two locally minimized configurations on the potential

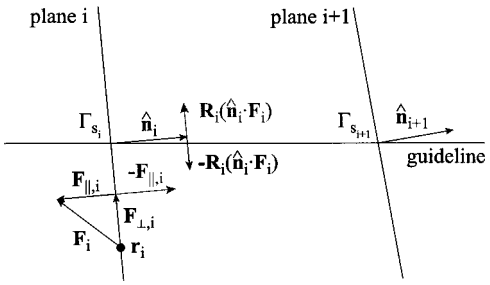

FIG. 3. An iteration in the progression of the hyperplane. Plane $i+1$ is found from the force acting on the system when it is confined to plane i. The force acting on the system in configuration $\mathbf{r_i}$, $\mathbf{F_i}=\mathbf{F}(\mathbf{r}_i)$, is divided into two components, $\mathbf{F}_{\perp,i}$ and $\mathbf{F}_{\parallel,i}$. The arm, $\mathbf{R}_i$, is defined by $\mathbf{R}_i=\mathbf{r}_i-\mathbf{\Gamma}_{s_i}$. The plane is translated along the path according to $-\mathbf{F}_{\parallel,i}$ and rotated about the intersection point $\mathbf{\Gamma}_{s_i}$ according to $\mathbf{R}_i(\mathbf{n}_i\cdot\mathbf{F}_i)$. The figure illustrates the calculation for a single configuration, $\mathbf{r_i}$, but the translation and rotation of the plane are based on canonical ensemble averages.

energy surface. A path, $\mathbf{\Gamma}_s$, is parametrized between the two minima, with a reaction coordinate s such that $\mathbf{\Gamma}_0=\mathbf{R}$ and $\mathbf{\Gamma}_1=\mathbf{P}$. $\mathbf{\Gamma}_s$ will be chosen here as the straight line connecting $\mathbf{R}$ and $\mathbf{P}$ in which case $\mathbf{\Gamma}_s=\mathbf{R}+s(\mathbf{P}-\mathbf{R})$. This line will henceforth be referred to as the guideline. The reactant and product regions in configuration space are R and P, respectively.

The system is confined to a hyperplane Z. The normal to the hyperplane is denoted by $\hat{\mathbf{n}}$. $\mathbf{\Gamma}_s$ is the point of intersection between the hyperplane and the guideline. The hyperplane is translated along the path and simultaneously rotated about $\mathbf{\Gamma}_s$ in a stepwise manner as shown in Figs. 2 and 3. This creates a progression of hyperplanes. Each hyperplane i, in the progression is characterized by s_i and $\hat{\mathbf{n}}_i$, and is given by the points in coordinate space that satisfy $Z_i=\{\mathbf{r}\in\mathbb{R}^N|\hat{\mathbf{n}}_i\cdot(\mathbf{r}-\mathbf{\Gamma}_{s_i})=0\}$.

The plane moves according to the translational and rotational force acting on it. The motion is described by the time evolution of s and $\hat{\mathbf{n}}_\mathbf{s}$. The direction of the forces is reversed so that the plane climbs up the free energy surface. Choosing the direction of the unit normal of the plane to be such that it points towards increasing s, i.e., $\hat{\mathbf{n}}_\mathbf{s}\cdot\hat{\mathbf{t}}_s>0$, where $\hat{\mathbf{t}}_s$ is the unit tangent to the path, and letting $F(s)$ denote the thermally averaged force acting on the system in the direction of the normal, $F_s=\langle\mathbf{F}_{\parallel,s}\rangle/m_s=\hat{\mathbf{n}}_s(\langle\mathbf{F}(\mathbf{r})\rangle\cdot\hat{\mathbf{n}}_s)/m_s$, the equation of motion for s is

$$\ddot{s}=-F_s. \tag{5}$$

Here m_s is the effective mass of the plane. We use the velocity Verlet algorithm,[16] involving both s and the corresponding velocity, v_s, for the numerical calculation,

$$s_{i+1}=s_i+\Delta t v_i-\tfrac{1}{2}\Delta t^2 F_i, \tag{6}$$

$$v_{i+1}=v_i-\frac{\Delta t}{2}(F_{i+1}+F_i), \tag{7}$$

where Δt is a time step for the plane progression. The choice of the mass of the plane will be explained later. In order to converge on the plane position where $F=0$, the equations of motion are modified by setting $v_i=0$ if $F_i v_i<0$, i.e., the velocity of the plane is zeroed if the plane has gone past the maximum free energy position.

The time evolution of the orientation of the hyperplane is given by an equation of motion for the unit normal, $\hat{\mathbf{n}}_\mathbf{s}$. The force acting to change the normal is $\tau_i=\langle(\hat{\mathbf{n}}_i\cdot\mathbf{F}_{\parallel,i})\mathbf{R}_i/\alpha_i|\mathbf{R}_i|^2\rangle$, where the arm, $\mathbf{R}_i$, is defined as $\mathbf{R}_i=\mathbf{r}-\mathbf{\Gamma}_{s_i}$, and $\alpha_i|\mathbf{R}_i|^2$ is the moment of inertia of plane i. The parameter α_i is chosen to control how fast the plane rotates. The choice of this parameter is discussed below. The equation of motion for the unit normal is

$$\ddot{\hat{\mathbf{n}}}_s=-\tau_s. \tag{8}$$

In the velocity Verlet form for a numerical integration, the equation of motion for the unit normal becomes

$$\hat{\mathbf{n}}_{i+1}=\mathbf{n}_i+\Delta t\omega_i-\tfrac{1}{2}\Delta t^2\tau_i, \tag{9}$$

$$\omega_{i+1}=\omega_i-\frac{\Delta t}{2}(\tau_{i+1}+\tau_i). \tag{10}$$

ω_i is the velocity vector giving the rate of change of the orientation of the plane, $\omega=d\hat{\mathbf{n}}/dt$. Equations (9) and (10) are equations of motion for a linearized rotation in N-dimensions, see Appendix A. The orientation of the plane is made to converge to the orientation at which $\tau=0$ by zeroing the rotational velocity when the plane has rotated beyond the zero force orientation, otherwise only the component of the velocity along the force is kept. That is, if $\tau_i\cdot\omega_i>0$, then ω_i is set to $\hat{\tau}_i(\omega_i\cdot\hat{\tau}_i)$, where $\hat{\tau}_i$ is the unit vector in the direction of τ_i, but otherwise ω_i is set to $\mathbf{0}$. Note that $\hat{\mathbf{n}}_{i+1}$ calculated from Eq. (9) must be normalized, since linearized rotation does not preserve magnitude, see Appendix A.

The first plane in the progression is chosen to be slightly away from the minimum corresponding to the reactants so that the force acting on the plane is nonzero. The first plane in the progression, therefore, has some finite value of $s>0$, say $s=s_1$. We typically choose $0.0<s_1<0.1$ and $\mathbf{r}=\mathbf{\Gamma}_{s_1}$ as a starting configuration of the system in the first plane. Later on, the free energy from this starting plane to the reactant minimum is evaluated. The force F_0 and the velocity v_0 in the first step are set to zero when evaluating v_1 in Eq. (7) and the vectors τ_0 and ω_0 are set to $\mathbf{0}$ in order to calculate ω_1 using Eq. (10).

Once the next position and orientation of the plane has been calculated, a thermal average of F and τ need to be evaluated again. A starting position of the system in the new plane corresponding to the average position in the previous plane can be obtained from

$$\mathbf{r}_{i+1}=\mathbf{\Gamma}_{s_{i+1}}+\mathbf{R}_{i+1}, \tag{11}$$

where

$$\mathbf{R}_{i+1}=\langle\mathbf{R}_i\rangle-\hat{\mathbf{n}}_i(\langle\mathbf{R}_i\rangle\cdot(\hat{\mathbf{n}}_{i+1}-\hat{\mathbf{n}}_i)). \tag{12}$$

The arm calculated from this equation should be adjusted so that $|\mathbf{R}_{i+1}|=|\langle\mathbf{R}_i\rangle|$, because the rotation should not effect the length of the arm. The initial coordinates of the system in a calculation of a thermal average is only important when the sampling is constrained to a subset of configuration space

because of a high barrier between one region and another. In order to obtain a free energy within the accessable subspace and get a smooth integration of the reversible work from one plane to another, the system needs to be started up in the same region of configuration space in the new plane.

Following is a summary of the algorithm for advancing the hyperplane:

Step 1: Calculate the thermal average of $\mathbf{F}_{\parallel,i}$ and τ_i in plane i;

Step 2: Calculate v_i from Eq. (7), using F_i and F_{i-1}, and then calculate s_{i+1} from Eq. (6);

Step 3: Obtain ω_i using Eq. (10), using τ_i and τ_{i-1}, and then $\hat{\mathbf{n}}_{i+1}$ from Eq. (9);

Step 4: Evaluate $\mathbf{R}_{i+1}$ by using Eq. (12);

Step 5: Repeat steps *1–4*, until the canonical ensemble averages of the forces F_s and τ_s acting on the plane are sufficiently small.

It can be useful to place an upper limit on the translation and rotation of the plane during the progression such that $\Delta s_i < \Delta s_{\max}(i)$ and $\Delta\theta_i < \Delta\theta_{\max}(i)$ to ensure that the free energy integration is smooth enough. The parameters α_i and m_i can be adjusted to ensure Δs_i and $\Delta\theta_i$ fall within those limits.

Our experience indicates the choice of the parameters m_i and α_i needed for Eqs. (6)–(10) can be based upon values that work at zero temperature. This is a quick calculation which leads to convergence of the plane to a saddle point. The values of m_i and α_i may need some tuning at very high temperature.

C. Refinement of the guideline

Using the same guideline for the whole plane progression may lead to slow or incomplete convergence of the hyperplane. This occurs particularly when the average position of the system is not near the guideline. In such cases a small rotational force calls for a large change in the s coordinate. Since we have not explicitly coupled s and $\hat{\mathbf{n}}$ in the equations of motion, the net force on the plane along s can become zero, resulting in no further changes in s, while the rotating force remains nonzero.

This problem can be fixed by shifting the guideline. After the force F changes sign for the first time, the guideline is updated at each step. The guideline is then taken to be the line going though the average position in the previous plane, $\langle \mathbf{r}_i \rangle$, in the direction of the normal $\hat{\mathbf{n}}_i$. This means the plane is from now on translated along the normal at each step.

When the guideline is changed, the rotational force may become too large. In such cases, one or more purely rotational steps at fixed s can be taken until the rotational force has dropped below the given tolerance.

D. Incorporation of symmetry

Transitions in crystals can be equivalent by symmetry. For example, in the Al adatom diffusion on the Al(100) surface, discussed below, there are four equivalent directions for the displacement of the atoms, irrespective of what the detailed mechanism of the transition is. If we wish to optimize a dividing surface for one of the transitions, then it may be necessary to eliminate the effect of the other symmetrically equivalent transitions. A single hyperplane is only going to be a good dividing surface for one of the transitions. Unless there is a large potential energy barrier between the potential energy troughs corresponding to the different processes, the system will tend to escape from the bottleneck region for one of the processes into a product basin of another process, thereby reducing the estimate of the free energy barrier. The OH-TST method will under such circumstances give some sort of an average dividing surface for the two processes. If a system has fourfold symmetry, then the optimal dividing surface for one of the transitions is related to the optimal dividing surface for another equivalent one by a 90° rotation about the C_4 axis.

When the system has n-fold symmetry about a given symmetry axis, a product states can have equivalent product states rotated by $2\pi/n$ about the axis. Letting $\mathbf{P}_i$, $i=1,...,n-1$, denote the minimum energy configurations of the equivalent product states, a set of unit vectors, $\hat{\mathbf{p}}_i$, $i=1,...,n-1$, pointing to those states are given by

$$\hat{\mathbf{p}}_i = \frac{\mathbf{P}_i - \mathbf{R}}{|\mathbf{P}_i - \mathbf{R}|}. \tag{13}$$

This symmetry can be used to restrict the configurational sampling of the system to include only one of the symmetrically equivalent regions of configuration space. Then, the hyperplane progression converges to a dividing surface for only one of the product states. Half-lines, l_i, originating at the reactant minimum energy configuration, $\mathbf{R}$, parallel to the unit vectors $\hat{\mathbf{p}}_i$ are defined as

$$l_i = \{\mathbf{r} \in \mathbb{R}^N | \mathbf{r} = \mathbf{R} + t\hat{\mathbf{p}}_i, t \geqslant 0\}, \quad i=1,...,n-1. \tag{14}$$

At every step during the thermal sampling, the distance of the configuration of the system, $\mathbf{r}$, from each of the half-lines l_i is calculated

$$d_i = d(l_i, \mathbf{r}) = \sqrt{|\mathbf{R}-\mathbf{r}|^2 - |(\mathbf{R}-\mathbf{r})\cdot\hat{\mathbf{p}}_i\hat{\mathbf{p}}_i|^2}. \tag{15}$$

If the configurational sampling is to be restricted to the part of configuration space which includes final state $\mathbf{P}_1$, then d_1 should be the smallest distance. If at a step j the distance d_1 turns out to be greater than any of the other d_i, $i=2,...,n-1$, say d_2, then a step back to $\mathbf{r}_{j-1}$ is taken and the increment revised so as to create a new point within the right subregion of phase space. For example, if a classical dynamics simulation based on the velocity Verlet algorithm is used to carry out the thermal sampling, then the velocity $\mathbf{v}_{j-1}$ is reflected about the mirror plane that reflects $\hat{\mathbf{p}}_1$ onto $\hat{\mathbf{p}}_2$. The normal of the reflection plane is in the direction of $\hat{\mathbf{p}}_1 - \hat{\mathbf{p}}_2$ and the reflected velocity $\mathbf{v}'_{j-1}$ is given by

$$\mathbf{v}'_{j+1} = \mathbf{v}_{j-1} - 2(\mathbf{v}_{j-1}\cdot\hat{\mathbf{q}}_{12})\hat{\mathbf{q}}_{12}, \tag{16}$$

where $\hat{\mathbf{q}}_{ij}$ is the normalized vector $\mathbf{q}_{ij}$ given by

$$\mathbf{q}_{12} = \hat{\mathbf{p}}_1 - \hat{\mathbf{p}}_2 - ((\hat{\mathbf{p}}_1 - \hat{\mathbf{p}}_2)\cdot\hat{\mathbf{n}})\hat{\mathbf{n}}, \tag{17}$$

and $\hat{\mathbf{n}}$ is the normal of the hyperplane being sampled. Since the new velocity vector needs to lie within the hyperplane, the part of $\hat{\mathbf{p}}_1 - \hat{\mathbf{p}}_2$ that is parallel to the hyperplane normal is subtracted out. The vector $\mathbf{q}_{ij}$ is normalized to preserve the

magnitude of $\mathbf{v}_{j-1}$. This reflection does not, on average, affect the total energy of the system during a velocity Verlet sampling of the hyperplane.

E. Integration of the free energy

The free energy integration is performed in a way that is analogous to Eq. (4). The reaction path is defined as the piecewise linear path that connects the thermally averaged configuration of the system, $\langle \mathbf{r} \rangle$, in adjacent planes in the progression. The rotation and translation of the hyperplane are performed independently of each other so the free energy of the rotation and translation can be integrated separately. The two integrals are

$$\Delta A_{\text{trans}}(t) = -\int_0^t \langle \mathbf{F}_{\parallel} \rangle_{t'} \cdot \frac{d\mathbf{\Gamma}'_t}{dt'} dt', \tag{18}$$

where t is the distance along the piecewise linear reaction path starting at the initial configuration $\langle \mathbf{r}_{s_1} \rangle$, and

$$\Delta A_{\text{rot}}(t) = \int_0^t \langle (\mathbf{F}_{\parallel} \cdot \hat{\mathbf{n}}) \mathbf{R} \rangle_{\theta'} \cdot \frac{d\hat{\mathbf{n}}'}{dt'} dt'. \tag{19}$$

During the optimization, the plane may move back and forth over the free energy ridge before it converges at the optimal plane. The system then typically slides considerably within the plane as the plane crosses the ridge. These kinds of jumps will make the integrands in Eqs. (18) and (19) discontinuous and the numerical evaluation of the integrals will have errors because the average position of the system changes too much between adjacent planes. This problem can be circumvented by selecting for the integration only those planes that are on the same side of the free energy ridge and ignore the ones on the other side. That is, only planes with an average force with the same sign as the average force in plane 1 are included in the integration. Another problem that may arise is that some planes may have a higher free energy than the optimal plane, which we can check after the optimal plane has been found, using Eqs. (18) and (19). This happens when the plane charges up a potential energy slope before it has rotated sufficiently. Those planes are likewise discarded. By applying this ''grooming'' of the planes in the progression, the free energy integration has worked well in the applications we have made as will be demonstrated in Sec. III.

F. The ratio of configuration integrals in the reactant region

In order to complete the evaluation of the rate constant, the prefactor needs to be evaluated. The configuration integral ratio, Q^{Z^R}/Q^R, can be calculated using classical dynamics of a single trajectory coupled to a thermal bath (for example the velocity Verlet algorithm including stochastic collisions[16]). We initially assume Z^R is a slice of width ϵ around the hyperplane $Z^R = \{\mathbf{r} \in R | \hat{\mathbf{n}}_{Z^R} \cdot (\mathbf{r} - \mathbf{\Gamma}_{Z^R}) = 0\}$. R stands for the reactant region, $\hat{\mathbf{n}}_{Z^R}$ is the normal to the plane, $\mathbf{\Gamma}_{Z^R}$ is some reference point in the plane, and $\mathbf{r}$ is a configuration of the atoms in the system. Let δ_ϵ represent the constraint that the system lies within the slice of width ϵ,

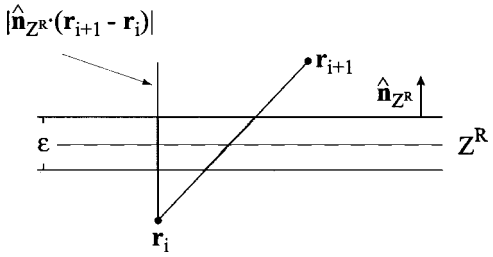

FIG. 4. Evaluation of the configuration integral ratio Q^{Z^R}/Q_R from a classical trajectory. A hyperplane Z^R is placed in the reactant region. The classical trajectory is used to calculate how much time the system spends in a slice of width ϵ around Z^R. The trajectory is assumed to be continuous and the slice thin enough that configurations $\mathbf{r}_{i+1}$ and $\mathbf{r}_i$ can be connected by a straight line segment. The amount of time the system spends in the slice is proportional to the fraction of the line segment $\mathbf{r}_{i+1}$ and $\mathbf{r}_i$ lying in the slice. The calculation of the ratio is done in terms of the projection onto the normal, $\epsilon / \mathbf{n}_{Z^R} \cdot (\mathbf{r}_{i+1} - \mathbf{r}_i)$.

$$\delta_\epsilon = \begin{cases} 1/\epsilon & \text{if } \mathbf{r} \text{ is in a slice of width } \epsilon \text{ around } Z^R \\ 0 & \text{otherwise.} \end{cases} \tag{20}$$

The function δ_ϵ is normalized in the direction of the normal and, therefore, has the value of $1/\epsilon$ everywhere in the hyperplane. The ratio can then be evaluated as

$$\frac{Q^{Z^R}}{Q^R} = \lim_{\epsilon \to 0} \frac{\int_R \delta_\epsilon [\hat{\mathbf{n}}_{Z^R} \cdot (\mathbf{r} - \mathbf{\Gamma}_{Z^R})] e^{-V_{Z^R}(\mathbf{r})/k_B T} d\mathbf{r}}{\int_R e^{-V(\mathbf{r})/k_B T} d\mathbf{r}} = \langle \delta_\epsilon \rangle. \tag{21}$$

The thermal average can be evaluated from a classical trajectory. The ensemble average δ_ϵ is proportional to the fraction of time the trajectory is in the slice. Whenever the classical trajectory crosses the hyperplane, i.e., when $\mathbf{r}_i$ is a configuration on one side of the plane and configuration $\mathbf{r}_{i+1}$ obtained one time step, Δt, later is on the other side of the plane, the two can be connected by linear interpolation and the time spent in the slice of width ϵ can be estimated from the fraction of the line segment that lies within the slice (as illustrated in Fig. 4). The time is $\Delta t \epsilon / |(\mathbf{r}_i - \mathbf{r}_{i+1}) \cdot \hat{\mathbf{n}}_{Z^R}|$. Here, the vector $\mathbf{r}_i - \mathbf{r}_{i+1}$ has been projected onto the normal $\hat{\mathbf{n}}_{Z^R}$ to evaluate δ_ϵ, the fraction of time spent in the slice needs to be multiplied by the value of δ_ϵ in the slice, $1/\epsilon$ and then the limit $\epsilon \to 0$ can be taken

$$\begin{aligned} \frac{Q^{Z^R}}{Q^R} &= \frac{1}{t_{\text{tot}}} \lim_{\epsilon \to 0} \frac{1}{\epsilon} \sum \frac{\Delta t \epsilon}{|(\mathbf{r}_i - \mathbf{r}_{i+1}) \cdot \hat{\mathbf{n}}_{Z^R}|} \\ &= \frac{\Delta t}{t_{\text{tot}}} \sum \frac{1}{|(\mathbf{r}_i - \mathbf{r}_{i+1}) \cdot \hat{\mathbf{n}}_{Z^R}|}. \end{aligned} \tag{22}$$

The sum is over pairs of points, $\mathbf{r}_i$ and $\mathbf{r}_{i+1}$, along the dynamical trajectory that are on opposite sides of the hyperplane, Z^R. During the simulation, it is possible to detect when the system crosses Z^R by noting when the dot product $\hat{\mathbf{n}}_{Z^R} \cdot (\mathbf{r}_{i+1} - \mathbf{\Gamma}_{Z^R})$ changes sign.

G. Calculation of the factor $\langle |v| \rangle$

The final contribution to the prefactor, $\langle |v| \rangle$, can be evaluated by integration,

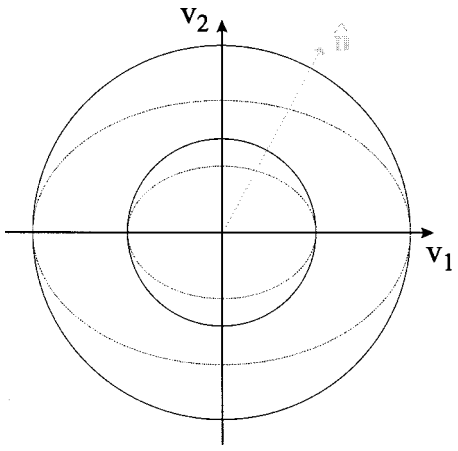

FIG. 5. An illustration of the calculation of the effective mass μ. Contour lines of the velocity distribution for coordinates of two particles, x_1 and x_2 are shown. The concentric circles represent the distribution if the mass of the two particles, m_1 and m_2, is the same. The elliptical curves represent the case when $m_2 > m_1$. The vector $\hat{\mathbf{n}}$ represents a direction for which one would like to determine the effective mass. Typically, $\hat{\mathbf{n}}$ is the normal to the transition state hyperplane.

$$\frac{\langle |v| \rangle}{2} = \frac{1}{2} \frac{\int_0^\infty v e^{-\mu v^2/2k_BT} dv}{\int_0^\infty e^{-\mu v^2/2k_BT} dv} = \sqrt{\frac{k_BT}{2\pi\mu}}. \tag{23}$$

Here μ is the effective mass for motion across the dividing surface in the direction of the normal,

$$\mu = \sum_i m_i (n_x^2 + n_y^2 + n_z^2). \tag{24}$$

The index i runs over all atoms in the system. This equation for μ can be derived by considering the Maxwell–Boltzmann distribution for velocity, illustrated in Fig. 5. For example, in a system of two particles, the velocity in the direction of a normalized vector, $\hat{\mathbf{n}} = (n_1, n_2)$, is given by $\mathbf{v} = v_1 \hat{\mathbf{x}}_1 + v_2 \hat{\mathbf{x}}_2$, where $v_1 = n_1 v$, and $v_2 = n_2 v$, v being the magnitude of $\mathbf{v}$. The probability distribution of velocity in any direction is proportional to $e^{-\mu v^2/k_BT}$, where μ is the effective mass for the direction. This distribution is also proportional to $e^{-(m_1 v_1^2 + m_2 v_2^2)/2k_BT} = e^{-(m_1 n_1^2 v^2 + m_2 n_2^2 v^2)/2k_BT}$, where m_1 and m_2 give the mass of the two particles. Comparing the two equivalent expressions for the velocity distribution shows $\mu = n_1^2 m_1 + n_2^2 m_2$. An extension to higher dimensions gives Eq. (24).

III. APPLICATIONS

The method has been applied to several two-dimensional systems, both to test and illustrate how the method works. The method has also been applied to a realistic, multidimensional system with several hundred degrees of freedom. It is, of course, most important that the method can be applied to complex, multidimensional systems.

In all calculations of canonical ensemble averages we use a single molecular dynamics trajectory. We simulate a system at a given temperature by applying stochastic collisions to the trajectory.[16]

A. Saddle points at $T = 0$ K

The method can be applied without much computational cost at $T = 0$ K since there is no need to evaluate a thermal average for each position of the hyperplane. The system then simply sits in a local potential energy minimum within the hyperplane. After the hyperplane has been moved the system is typically not at a minimum and it relaxes to the closest minimum energy configuration. As the hyperplane is pushed uphill and rotated against the force acting on it, the hyperplane will reach the top of and be aligned with the potential ridge. There the system is at a local minimum within the hyperplane and a local maximum in the direction of the normal to the hyperplane. The system will, therefore, end up sitting at a first order saddle point. However, since the system does not explore the region around the saddle point, and all derivatives of the potential are zero at the saddle point, the orientation of the plane is not well defined in the $T = 0$ K case. In the calculations presented in this section, the system was simulated at a very low temperature, $k_BT = 10^{-7} E^A$, where E^A is the energy of the saddle point with respect to $\mathbf{R}$.

Figure 6 shows the hyperplane progression in four different two-dimensional systems (here the hyperplane reduces to a line). The form of the potential function in each case is a LEPS potential coupled to a harmonic potential, with the addition of some Gaussians in (b)–(d). The LEPS part of the potential describes a three atom system where the atoms lie on a line and the central atom (atom B) can form one bond either with the atom to the left (atom A) or the atom to the right (atom C). A fourth atom, D, is coupled in a harmonic way to the central atom, B. The functional form and parameters are given in Appendix B. The initial guideline for advancing the hyperplane is a straight line that connects R and P. As the hyperplane moves up the slope, it rotates and eventually converges to an optimal hyperplane, denoted by ‡.

It serves as a good check on the numerical integration of the reversible work to calculate the integral at $T = 0$ K because the integrated reversible work should then equal the potential energy difference between the initial state and the saddle point. The reaction coordinate is the piecewise linear path connecting the minimum energy configuration of the system in each hyperplane. The result of the integration is shown in Fig. 7(a). The integrated reversible work is almost identical to the potential energy difference, as it should be. The integral was evaluated by using the trapezoidal rule, where the average value of the force for two adjacent planes was calculated and multiplied by the increment in the reaction coordinate. A higher order integration scheme could give more accurate integral and allow for a coarser progression of planes.

The translational and rotational force acting on the hyperplane at each position illustrate how convergence is reached. As shown in Fig. 7(b), the translational and rotational force increase as the plane climbs up the potential surface and reach a maximum near the inflection point of the potential energy curve. Then, the forces decrease and become negligible at the converged hyperplane.

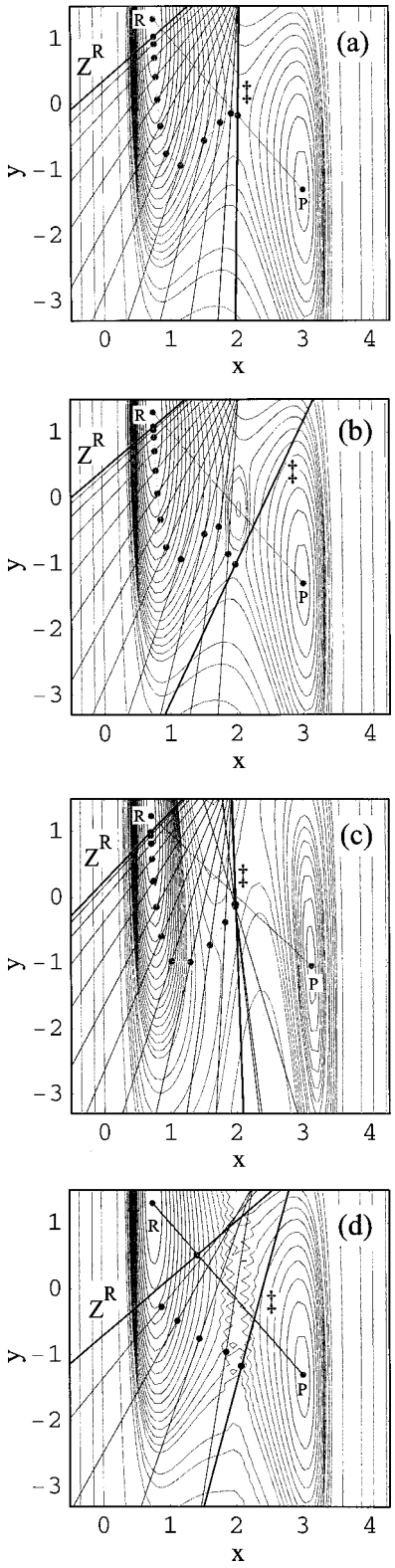

FIG. 6. Calculation of an optimal hyperplane at $T=0$ K. After convergence is reached the plane includes a saddle point on the potential energy surface. The hyperplane progression for four two-dimensional potentials is shown, (a)–(d). Z^R is the initial plane and the optimized plane is labeled with ‡. The initial guideline is the straight line connecting R and P. The plane progression is shown as a series of lines. Not all the planes used in the calculation are shown. The filled circle in each plane shows the configuration of the system. It is essential for the hyperplane to rotate in order to reach convergence, but the final orientation of the plane is not well defined because only the minimum energy configuration of the system within the plane is sampled.

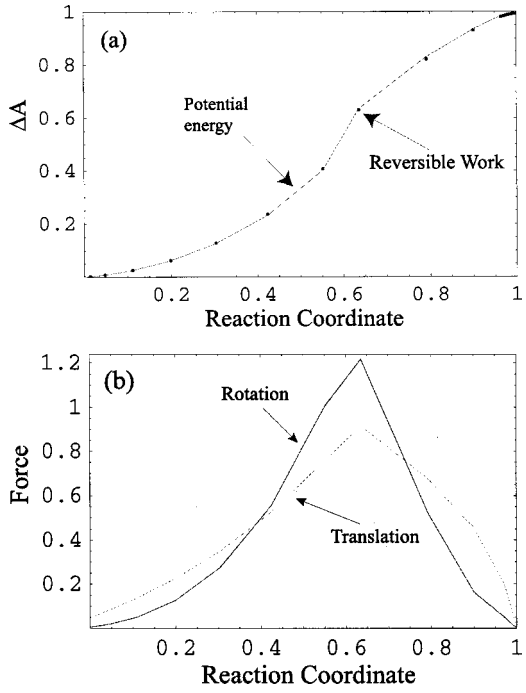

FIG. 7. (a) The integrated reversible work (shown with dots) at $T=0$ K along the reaction coordinate for the potential energy surface shown in Fig. 6(a). The integration starts from plane Z^R. The full curve is the potential energy difference along the same reaction coordinate. The agreement between the two illustrates the accuracy of the integration procedure. (b) The translational and rotational force acting on the planes in the plane progression shown in Fig. 6(a).

B. Free energy barriers at finite temperature

The two-dimensional potential surface V_a shown in Fig. 6(a) was used to calculate the free energy barrier at a temperature of $k_BT=0.1E^A$. The plane progression is shown in Fig. 8(a). This progression is similar to the one obtained at $T=0$ K [Fig. 6(a)], except that the optimal dividing surface is better aligned with the potential energy ridge in the finite temperature case. This is due to better sampling of the region around the saddle point at finite temperature.

It is important to allow the hyperplane to rotate. For comparison, Fig. 8(b) shows a plane progression where the orientation is kept fixed. This is the way free energy barriers are often calculated. Figure 8(c) illustrates how the lack of orientational optimization can affect the calculated free energy barrier. Without the rotation, the calculated free energy barrier is about 25% lower, corresponding to a 20 times larger rate than the orientationally optimized transition state gives.

The prefactor was also evaluated for the transition shown in Fig. 8(a). The ratio of the configuration integrals, $Q^{\ddagger}/Q^{Z^R}$ was found to be 0.765 ± 0.005 for V_a at $k_BT=0.1E^A$. The value of $\langle|v|\rangle$ was found to be 0.399, so the rate constant is estimated to be $k^{\text{OH-TST}}=(4.5\pm0.2)\times10^{-7}$. For comparison the exact rate calculated using the hyperdynamics method[17] and a flat bias potential[18] gave the value $k^{\text{TST}}=(4.4\pm0.1)\times10^{-7}$.[19]

This system is, in fact, simple enough that harmonic TST gives a very similar value for the rate constant $k^{\text{hTST}}=4.3\times10^{-7}$.

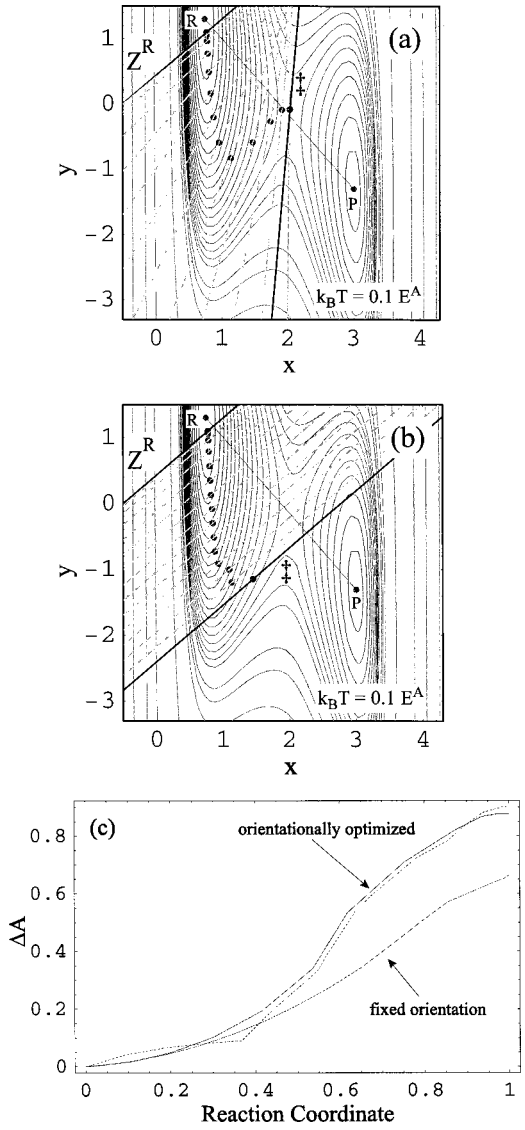

FIG. 8. (a) A reversible work calculation at a finite temperature, $k_BT = 0.1E^A$, for the potential energy surface shown in Fig. 6(a). The initial plane is Z^R and the optimized one is ‡. (b) Same as in (a), except the orientation of the plane is not allowed to change, as is often done in free energy calculations. (c) A comparison of the calculated free energy for the two plane progressions shown in (a) and (b). This illustrates the importance of including rotation of the plane. The dashed line shows the result of a free energy calculation when small ripples (a set of sinusoidal functions) have been added to the potential energy surface. The value of the free energy is not affected significantly but, since the potential surface now has ripples and multiple saddle points in the transition region, as shown in Fig. 9, harmonic TST would fail in this case.

However, it is easy to construct a potential surface where harmonic TST is not adequate. For example, adding a sheet of two-dimensional sinusoidal waves on top of the V_a potential, of the form $0.0025\sin(80x)\sin(80y)$ gives a surface which is essentially the same as V_a but now has small ripples. Figure 9 shows the slice of the potential surface that lies within the optimal transition state. The ripples strongly effect the harmonic TST estimate of the transition rate, but this is a failure of the harmonic approximation. The ripples here are small enough that the rate is not significantly effected. The free energy curve obtained from the reversible work calculation is shown in Fig. 8(c) and is close to the original results, without the ripples. This example illustrates that the OH-TST calculation can, in principle, be applied to complex systems where the location of the transition state dividing surface cannot simply be inferred from the location of a saddle point on the potential energy surface.

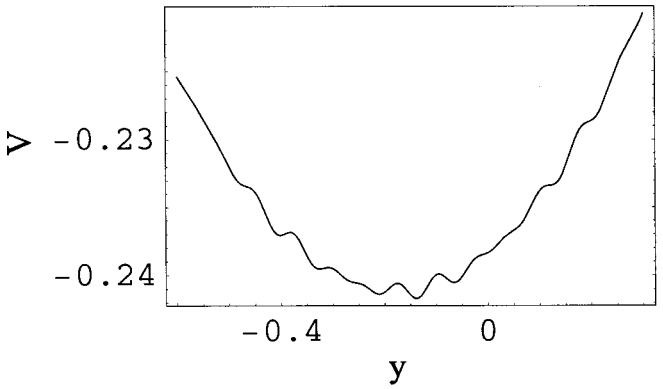

FIG. 9. The potential energy within an optimal hyperplanar dividing surface for a potential constructed by adding sinusoidal ripples to the potential surface shown in Fig. 8(a). This potential surface has multiple saddle points in the transition region. The free energy curve obtained by the reversible work integration is shown in Fig. 8(c).

C. Symmetric Eckart barrier

An optimization of the dividing surface for the two-dimensional Eckart barrier has been presented by Makarov and Metiu.[6] They carried out a direct calculation of the rate constant for various dividing surfaces. The potential energy is given by

$$V_{\text{Eckart}}(x,y) = \frac{V_0}{\cosh^2\left(\frac{\alpha x}{2}\right)} + \frac{1}{2}\mu\omega^2(y - Cx)^2, \tag{25}$$

with $V_0 = 0.0156$, $\alpha = 3.97$, $\frac{1}{2}\mu\omega^2 = 1.04\times10^{-4}$, and $C = 10$. A contour plot of the potential is shown in Fig. 10.

Makarov and Metiu tested several dividing surfaces going through $(x,y) = (0,0)$ by varying the orientation of the dividing surface. The smallest rate was found at an angle of 0° with respect to the y-axis at $k_BT = 0.1E^A$, parallel to the potential energy ridge at $x = 0$. At higher temperature, $k_BT = 0.3E^A$, the best dividing surface had a much larger tilt from the y-axis, about 70°.[20] There is a large number of recrossings of the dividing surface in this system, especially at the higher temperature. Makarov and Metiu found that the best diving surface is not the one minimizing the number of recrossings.[6]

We carried out OH-TST calculations, first by constraining the dividing surface to go through (0, 0), and found optimal orientation in good agreement with the results of Makarov and Metiu, both at the low and high temperature (1° at low T and 74° at high T). A full optimization of the dividing surface, both location and orientation, gave the results shown in Fig. 10. Here, the optimal dividing surface has moved slightly away from $(x,y) = (0,0)$. In this calculation, the configurations **R** and **P** were chosen to be the minimum

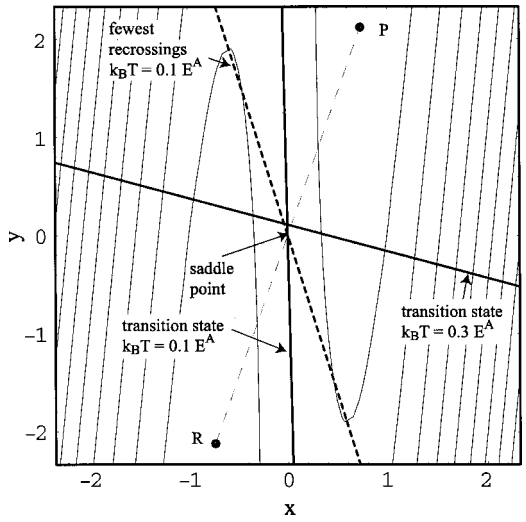

FIG. 10. Optimal dividing surfaces, corresponding to maximum free energy, for the two-dimensional Eckart barrier at low ($k_BT=0.1E^A$) and high ($k_BT=0.3E^A$) temperature. The plane leading to fewest recrossings at the lower temperature is shown with a thick dashed line (Refs. 6, 20) and is clearly different from the plane with maximum free energy.

energy configurations in a slice of the potential parallel to the *x*-axis (there is not a stable minimum energy configuration on this potential surface).

At the higher temperature, the average kinetic energy is a considerable portion of the barrier height. The basic assumptions of TST may not apply in such cases as the transition is not slow. The OH-TST method, nevertheless, converges in this case to an optimal dividing surface which agrees closely with the dividing surface obtained by direct rate calculations.

D. Al adatom diffusion on Al(100)

The most important question is how well the OH-TST algorithm performs in high dimensional problems. We applied the method to Al adatom diffusion on a Al(100) surface. The system is simulated as a slab of 6 Al layers with 50 atoms in each layer. The atoms in the two lowest layers were kept fixed. An adatom was placed on the surface in the stable, fourfold hollow site. The system therefore consists of 201 atoms, or 603 degrees of freedom.

The transition of interest is the diffusion of the adatom on the surface. The simplest mechanism for diffusion is a hop over the bridge site (see Fig. 11). This was the assumed mechanism until Feibelman carried out density functional theory (DFT) calculations of the energetics of various transition mechanisms and found that a two-atom concerted displacement mechanism is lower in energy (see Fig. 11).[21] Both mechanisms result in a diffusion of an adatom on the surface, but the final state of the two transitions is quite different.

The calculations presented here make use of an embedded atom method (EAM) potential surface of the Voter–Chen form.[22] The calculated energy barrier for the concerted displacement process is 0.23 eV and 0.37 eV for the hop, in quite good agreement with the DFT calculations. The results of OH-TST calculations at $T=210$ K are shown in Fig. 12.

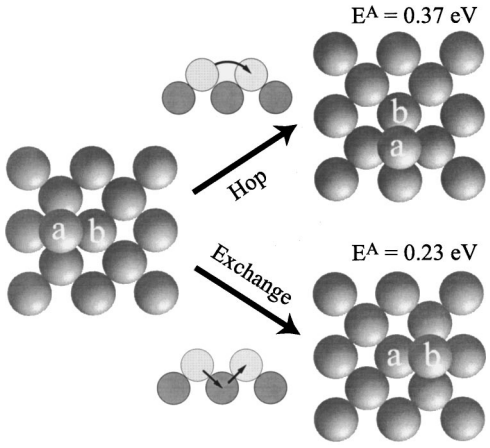

FIG. 11. Two different diffusion mechanisms for an Al adatom on an Al(100) surface, the hop and two-atom concerted displacement. The concerted displacement (''exchange'') process has lower activation energy. Note that the final state is quite different in the two processes.

Results of two calculations of the free energy barrier for the concerted process are given, the only difference being the parameter determining the moment of inertia of the hyperplane and the maximum angle of rotation in a single step. These values were 0.00473 and 5° in one case, and 0.0141 and 1° in the other. The free energy rises faster in the case where the hyperplane rotates faster. The difference in the calculated free energy barrier is less than the error bar associated with the numerical calculation.

Figure 12 also shows the results of a calculation where the initial guideline was drawn from the initial state to the final state of the hop mechanism. However, during the plane progression the hyperplane rotated enough that it converged on an optimal hyperplanar dividing surface for the concerted displacement process. This was verified by minimizing configurations from several locations within the transition state

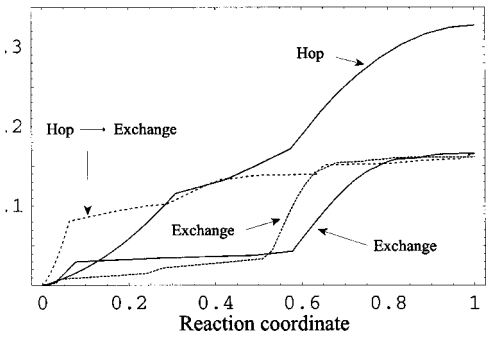

FIG. 12. Free energy curves at $T=210$ K for the hop and concerted displacement (''exchange'') mechanism of Al adatom diffusion (see Fig. 11). The free energy barrier for the concerted displacement mechanism is found to be 0.16 eV while the hop has free energy barrier of 0.33 eV. Two calculations of the free energy barrier for the concerted displacement process are shown. The dashed lines correspond to calculations with three times smaller moment of inertia than the solid lines. The dashed line farthest to the left shows results of calculation where the guiding line is that of the hop mechanism, but the hyperplane converges to the transition state of the concerted displacement mechanism, which has lower free energy barrier. When the moment of inertia is too large, the plane is unable to rotate enough to find the concerted displacement. This demonstrates how OH-TST can reveal the optimal transition mechanism even when the method is started up with a guideline corresponding a different, less than optimal mechanism.

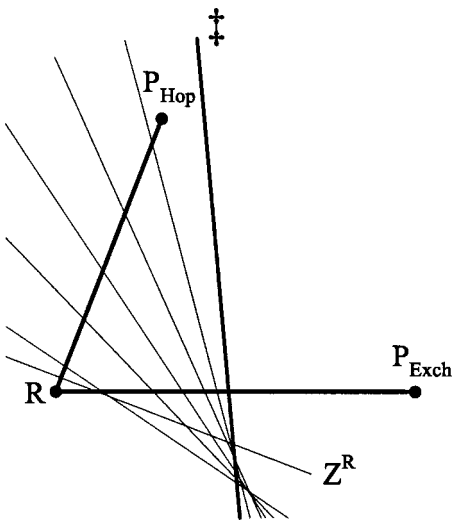

FIG. 13. An illustration of how OH-TST locates a free energy barrier for the concerted displacement mechanism when the calculation is started out with a guideline tailored to the hop mechanism. The filled circles represent minimum energy configurations in the reactant region (**R**), the product region for the hop ($\mathbf{P}_{\mathrm{Hop}}$), and the product region for the concerted displacement ($\mathbf{P}_{\mathrm{Exch}}$). The angle between $\mathbf{P}_{\mathrm{Hop}}-\mathbf{R}$ and $\mathbf{P}_{\mathrm{Exch}}-\mathbf{R}$ and their relative magnitudes in the figure are the same as in the actual system. The hyperplanes in the progression are projected onto the two-dimensional space spanned by the two vectors $\mathbf{P}_{\mathrm{Hop}}-\mathbf{R}$ and $\mathbf{P}_{\mathrm{Exch}}-\mathbf{R}$. The projection of each hyperplane is calculated by determining the interception point of the plane with lines through **R** and along $\mathbf{P}_{\mathrm{Hop}}-\mathbf{R}$ and $\mathbf{P}_{\mathrm{Exch}}-\mathbf{R}$. The optimal transition state is labeled with ‡. Not all planes in the progression are shown.

hyperplane. 38% of the trajectories ended up in the final state for the concerted displacement, and 62% trajectories ended up in the initial state. No trajectory ended up in the final state for hop. This illustrates how the orientational optimization makes the method flexible enough to be able to identify an unexpected, optimal mechanism even when the calculation is started up with a guideline for a different mechanism.

Figure 13 shows a schematic explanation of how this occurs. The plane progression is represented in a two-dimensional space. This two-dimensional space is spanned by the vectors $\mathbf{P}_{\mathrm{Hop}}-\mathbf{R}$ and $\mathbf{P}_{\mathrm{Exch}}-\mathbf{R}$, where **R** is the minimum energy configuration in the reactant region, $\mathbf{P}_{\mathrm{Hop}}$ is the minimum energy configuration in the product region of the hop, and $\mathbf{P}_{\mathrm{Exch}}$ is the minimum energy configuration in the product region of the concerted displacement. The projection of $\mathbf{P}_{\mathrm{Exch}}-\mathbf{R}$ is chosen to lie on the *x*-axis pointing in the positive direction. The angle between $\mathbf{P}_{\mathrm{Hop}}-\mathbf{R}$ and $\mathbf{P}_{\mathrm{Exch}}-\mathbf{R}$ is $\arccos\left((\mathbf{P}_{\mathrm{Exch}}-\mathbf{R})\cdot(\mathbf{P}_{\mathrm{Hop}}-\mathbf{R})/|\mathbf{P}_{\mathrm{Exch}}-\mathbf{R}||\mathbf{P}_{\mathrm{Hop}}-\mathbf{R}|\right)=69°$. The projections of the hyperplanes in the progression are given by the lines in Fig. 13, as shown in Appendix C. At first, the plane progression heads towards the free energy barrier for the hop mechanism. At some point the system in the plane has enough energy to escape from the valley that leads to the hop into the valley leading to the concerted displacement.

When the moment of inertia of the hyperplane is increased enough, to 0.154 from 0.00220 in the calculation described above, the rotation is limited enough that the OH-TST calculation converges on a transition state for the hop. This was verified by minimizing several images of the system within the transition state hyperplane. 41% of the images

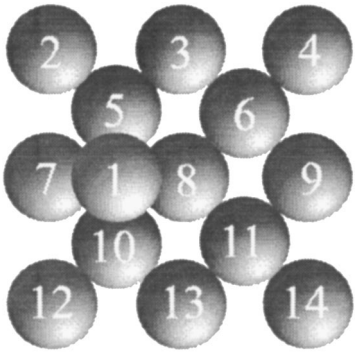

FIG. 14. Al adatom in a stable position on the Al(100) surface (the initial state for diffusion). The atoms are numbered to aid the discussion of the reaction coordinates (see text).

ended up in the final state for hop, and 59% images ended up in the initial state. No image ended up in the final state for concerted displacement.

The OH-TST calculations gave a free energy barrier for the concerted displacement of 0.16 eV and a barrier of 0.33 eV for the hop. The entropic effects within the hyperplane are larger for the concerted displacement, reducing the barrier by 30% as compared with 11% for the hop. The transition states are quite different, and apparently the transition state for the concerted displacement, where the adatom has been driven into the surface, has higher entropy.

The direction of the hyperplane normal at the transition state represents an optimal choice for the reaction coordinate for the transition, in that region of configuration space, since the hyperplane is a tangent surface to the full dividing surface. The normal can be written as $\hat{\mathbf{n}}=\{\hat{\mathbf{n}}_1,\hat{\mathbf{n}}_2,\ldots,\hat{\mathbf{n}}_N\}$, where each $\hat{\mathbf{n}}_i$ is a three-dimensional vector corresponding to each atom and *N* is the number of atoms in the system. Atoms with the largest $\hat{\mathbf{n}}_i$ are the atoms that contribute most to the reaction coordinate. This can, for example be used to characterize the hop and concerted displacement mechanisms in Al diffusion. Giving only the magnitude of the displacement of each atom in a format $i(|\hat{\mathbf{n}}_i|)$, with *i* as the atom number (see Fig. 14), the concerted displacement mechanism has a reaction coordinate {1(0.667), 8(0.592), 10(0.108), 6(0.083), 11(0.073), 5(0.071), 9(0.070)} while the hop mechanism is {1(0.973), 8(0.078), 10(0.078), 11(0.046), 13(0.046)}. The processes are shown in Fig. 11.

The thermal sampling within the hyperplane was reduced by making use of the fourfold symmetry in all the Al diffusion calculations as described in Sec. II D. Without the symmetry constraint, the OH-TST calculations converged to a hyperplane that resembled an average plane for two symmetrically equivalent concerted displacement processes.

IV. SUMMARY

The method presented here, OH-TST, can be used to find in a systematic way the optimal hyperplanar dividing surface for a TST estimate of a rate constant. The optimization is naturally built into the reversible work evaluation of the free energy barrier. The method can, in principle, be applied to large and complex systems. At $T=0$ K the method locates saddle points. At finite temperature, the method can find an

optimal dividing surface for highly anharmonic systems, involving many saddle points, where the harmonic approximation TST is not applicable. The method can also work where entropic effects dominate and the optimal dividing surface is not near a saddle point, as was illustrated with the Eckart barrier test problem.

OH-TST may be used to predict mechanisms of slow transitions. An analysis of Al adatom diffusion on Al(100) surface showed that the method is able to find a mechanism with lower free energy barrier than the one used to start the calculation. A limitation of OH-TST in that study was the hyperplanar representation of the dividing surface which breaks down at temperatures higher than 210 K because the system can escape away from the bottleneck region even though it is confined within the hyperplane. A possible solution to this problem is to construct a piecewise hyperplanar dividing surface. When the system visits a boundary of two hyperplanes it is either reflected back and kept in the same hyperplane or it is reflected into the hyperplane on the other side of the boundary. This is illustrated in Fig. 1. Hyperplane h_2 is used to represent the dividing surface between R and P_5. At some temperature, the system confined to h_2 will be able to escape from the bottleneck region connecting R and P_5 into product region P_4. By using two hyperplanes, h_2 and h_3, to represent the dividing surface, h_2 in the region between R and P_5 and h_3 in the region between R and P_4, this problem could be avoided. Another possibility is to generalize the method to curved dividing surfaces.

ACKNOWLEDGMENTS

We would like to thank Graeme Henkelman for helpful suggestions and discussions. This work was funded by National Science Foundation, Grant No. CHE-9710995, and by the Petrolium Research Fund, Grant No. PRF32626-AC5/REF104788.

APPENDIX A

The orientation of the hyperplane is adjusted at each step in the plane progression. The normal is rotated in a two-dimensional plane, regardless of the dimensionality of the system.[9] Consider an arbitrary N-dimensional vector $\mathbf{y}$. Assume that $\mathbf{y}$ is rotated about an angle θ. For pure rotation, we can choose a basis set for $\mathbf{y}$ such that the rotation occurs in a two-dimensional subspace of the N-dimensional space. In other words, the rotation affects only two coordinates of $\mathbf{y}$ in this basis. The rotation is perpendicular to the remaining coordinates. Let us assume that $\mathbf{y}$ is rotated in the $(\mathbf{b}_1,\mathbf{b}_2)$-plane, as illustrated in Fig. 15(a).

The projection of $\mathbf{y}$ onto the $(\mathbf{b}_1,\mathbf{b}_2)$-plane is the vector $\mathbf{y}_p$. The rotation can be accomplished by adding a vector $\Delta\mathbf{y}$ ($\Delta\mathbf{y}$ is perpendicular to $\mathbf{y}_p$) to $\mathbf{y}_p$. The resulting vector, $\mathbf{y}_r$, must be scaled such that $|\mathbf{y}_r|=|\mathbf{y}_p|$. Finally $\mathbf{y}_r$ is added to the part of $\mathbf{y}$ that was not projected onto the $(\mathbf{b}_1,\mathbf{b}_2)$-plane, to get the rotated image of $\mathbf{y}$.

Figure 15(b) illustrates how the normal of a hyperplane is rotated during the plane progression. The normal component of the force, $\mathbf{F}_\parallel=\mathbf{F}\cdot\hat{\mathbf{n}}$, acts on the hyperplane at a point located at $\mathbf{R}$ from the turning point. This causes a rotational force, τ, which acts to rotate the normal of the hyperplane in the plane formed by the arm, $\mathbf{R}$, and the normal, $\hat{\mathbf{n}}$. The magnitude of the rotational force is $|\tau|=|\mathbf{R}||\mathbf{F}_\parallel|$ and the direction of τ is such as to oppose the force acting on the plane (thus rotating the plane to higher free energy). This gives

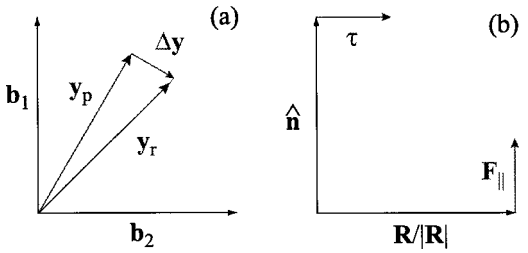

FIG. 15. An illustration of the calculation of the rotation of the hyperplane. (a) The rotation of the normal occurs in a two dimensional plane spanned by basis vectors $\mathbf{b}_1$ and $\mathbf{b}_2$. (b) The two basis vectors can be taken to be a unit vector in the direction of the arm $\mathbf{R}$ and the plane's normal, $\hat{\mathbf{n}}$. The vector τ gives the change in the direction of the normal. The plane rotates against the rotational force acting on it by adding $\tau=\mathbf{R}(\hat{\mathbf{n}}\cdot\mathbf{F})$ to the normal.

$$\tau=\frac{\mathbf{R}}{|\mathbf{R}|}|\mathbf{R}||\mathbf{F}_\parallel|\mathrm{sign}(\hat{\mathbf{n}}\cdot\mathbf{F})=\mathbf{R}(\hat{\mathbf{n}}\cdot\mathbf{F}). \tag{A1}$$

APPENDIX B

The two-dimensional potentials used in the test calculations shown in Figs. 6(a)–6(d) are based on a LEPS plus harmonic oscillator potential, V_{LEPSpHO}, shown in Fig. 6(a). The LEPS potential describes the interaction of three atoms A, B, and C where only one "bond" can be formed,[23]

$$\begin{aligned}V_{\mathrm{LEPS}}(r_{\mathrm{AB}},r_{\mathrm{BC}})=&\frac{Q_{\mathrm{AB}}}{1+a}+\frac{Q_{\mathrm{BC}}}{1+b}+\frac{Q_{\mathrm{AC}}}{1+c}-\Bigg[\frac{J_{\mathrm{AB}}^2}{(1+a)^2}\\&+\frac{J_{\mathrm{BC}}^2}{(1+b)^2}+\frac{J_{\mathrm{AC}}^2}{(1+c)^2}\\&-\frac{J_{\mathrm{AB}}J_{\mathrm{BC}}}{(1+a)(1+b)}-\frac{J_{\mathrm{BC}}J_{\mathrm{AC}}}{(1+b)(1+c)}\\&-\frac{J_{\mathrm{AB}}J_{\mathrm{AC}}}{(1+a)(1+c)}\Bigg]^{1/2},\end{aligned} \tag{B1}$$

where the Q functions represent Coulomb interactions between the electron clouds and the nuclei and the J functions represent the quantum mechanical exchange interactions. These functions are

$$Q(r)=\frac{d}{2}\left(\frac{3}{2}e^{-2\alpha(r-r_0)}-e^{-\alpha(r-r_0)}\right), \tag{B2}$$

and

$$J(r)=\frac{d}{4}(e^{-2\alpha(r-r_0)}-6e^{-\alpha(r-r_0)}). \tag{B3}$$

The parameters used in the calculations presented here are $a=c=0.05$, $b=0.80$, $r_{0,\mathrm{AB}}=r_{0,\mathrm{BC}}=r_{0,\mathrm{AC}}=0.742$, $\alpha_{\mathrm{AB}}=\alpha_{\mathrm{BC}}=\alpha_{\mathrm{AC}}=1.942$, $d_{\mathrm{AB}}=d_{\mathrm{BC}}=4.746$, and $d_{\mathrm{AC}}=3.445$. The LEPS potential is used here in such a way that the position of the end atoms A and C is fixed and only atom B is allowed to move.

A second degree of freedom is added to the LEPS potential. This can be interpreted as a fourth atom, D, coupled to atom B in a harmonic way,

$$V_{\mathrm{LEPSpHO}}(x,y)=V_{\mathrm{LEPS}}(x,r_{\mathrm{AC}}-x) + 2k_c(x-(r_{\mathrm{AC}}/2-y/c))^2, \tag{B4}$$

where $k_c=0.2025$, $r_{\mathrm{AC}}=3.742$, and $c=1.154$. A contour plot of this potential is shown in Fig. 6(a).

The potentials shown in Figs. 6(b)–6(d) were constructed by adding $V'(x,y)$ to the $V_{\mathrm{LEPSpHO}}(x,y)$ potential,

$$V_i(x,y)=V_{\mathrm{LEPSpHO}}(x,y)+V_i'(x,y), \tag{B5}$$

where $i=b,c,d$. The form of the $V'(x,y)$ functions was

$$V_b'(x,y)=1.5G(x;2.02083,0.1)G(y;-0.172881,0.35), \tag{B6}$$

$$V_c'(x,y)=2(G(x;1.6,0.3)E(y;-2.0,0.5) + G(x;2.4,0.3)E(y;2.0,-0.5)), \tag{B7}$$

$$V_d'(x,y)=0.3G(x;C(y),0,1), \tag{B8}$$

where the G, E, and C functions are defined as

$$G(r;r_0,\sigma_r)=e^{-(r-r_0)^2/2\sigma_r^2}, \tag{B9}$$

$$E(r;r_0,\alpha_r)=e^{\alpha_r(r-r_0)}, \tag{B10}$$

$$C(y)=2.02083+0.1\cos[10\pi(y+0.172881)]. \tag{B11}$$

The coordinate $(x,y)=(2.020\,83,-0.172\,881)$ corresponds to the first order saddle point on the V_{LEPSpHO} surface.

APPENDIX C

In Sec. III D the hyperplanes in the plane progression leading to the free energy barrier for the concerted displacement process were projected onto a two-dimensional space spanned by the vectors $\mathbf{P}_{\mathrm{Hop}}-\mathbf{R}$ and $\mathbf{P}_{\mathrm{Exch}}-\mathbf{R}$. Here it is shown that this projection gives a line for each of the hyperplanes.

A point $\mathbf{r}$ in this two-dimensional coordinate system can be expressed by $\mathbf{r}=\alpha\hat{\mathbf{p}}_{\mathrm{Hop}}+\beta\hat{\mathbf{p}}_{\mathrm{Exch}}$ with $\hat{\mathbf{p}}_{\mathrm{Hop}}=\mathbf{P}_{\mathrm{Hop}}-\mathbf{R}|\mathbf{P}_{\mathrm{Hop}}-\mathbf{R}|$, $\hat{\mathbf{p}}_{\mathrm{Exch}}=\mathbf{P}_{\mathrm{Exch}}-\mathbf{R}|\mathbf{P}_{\mathrm{Exch}}-\mathbf{R}|$, and α and β some real numbers. Therefore, the set of all points in the two-dimensional system is given by $\{\mathbf{r}\in\mathbb{R}^{3N}|\alpha\hat{\mathbf{p}}_{\mathrm{Hop}}+\beta\hat{\mathbf{p}}_{\mathrm{Exch}}=\mathbf{r}\forall\,\alpha,\beta\in\mathbb{R}\}$. All points $\mathbf{r}$ in a hyperplane satisfy the condition $\hat{\mathbf{n}}\cdot(\mathbf{\Gamma}-\mathbf{r})=0$, with $\hat{\mathbf{n}}$ the plane's normal and Γ a reference point in the plane. Thus the set of all points in a hyperplane is given by $\{\mathbf{r}\in\mathbb{R}^{3N}|\hat{\mathbf{n}}\cdot(\mathbf{\Gamma}-\mathbf{r})=0\}$. From the OH-TST calculation we have $\hat{\mathbf{n}}$ and $\mathbf{\Gamma}$ for all the planes in the progression. The hyperplanes in the plane progression have a single interception point with each of the two lines l_{Hop}:$\{\alpha\in\mathbb{R}|\mathbf{R}+\alpha\hat{\mathbf{p}}_{\mathrm{Hop}}\}$ and l_{Exch}:$\{\alpha\in\mathbb{R}|\mathbf{R}+\alpha\hat{\mathbf{p}}_{\mathrm{Exch}}\}$. This is evident by noting that $\hat{\mathbf{n}}\cdot(\mathbf{\Gamma}-\mathbf{r})=0$ changes sign when going along either line l_{Hop} or l_{Exch}.

We now show that the projection of a hyperplane onto the two-dimensional space spanned by $\mathbf{P}_{\mathrm{Hop}}-\mathbf{R}$ and $\mathbf{P}_{\mathrm{Exch}}-\mathbf{R}$ is indeed the line through the two interception points of the plane with the lines l_{Hop} and l_{Exch}. The problem is to find the intersect between the two sets, $\{\mathbf{r}\in\mathbb{R}^{3N}|\hat{\mathbf{n}}\cdot(\mathbf{\Gamma}-\mathbf{r})=0\}$ and $\{\mathbf{r}\in\mathbb{R}^{3N}|\alpha\hat{\mathbf{p}}_{\mathrm{Hop}}+\beta\hat{\mathbf{p}}_{\mathrm{Exch}}=\mathbf{r}\forall\,\alpha,\beta\in\mathbb{R}\}$. Assuming the hyperplane's normal is not perpendicular to both $\hat{\mathbf{p}}_{\mathrm{Hop}}$ and $\hat{\mathbf{p}}_{\mathrm{Exch}}$, the space spanned by the two-dimensional coordinate system cannot be a subset of the hyperplane. Since the intercepts are points on the lines l_{Hop} and l_{Exch}, given by, say, $\alpha=\alpha_1$ and $\alpha=\alpha_2$ respectively, we can write

$$\hat{\mathbf{n}}\cdot(\mathbf{\Gamma}-\mathbf{R}-\alpha_1\hat{\mathbf{p}}_{\mathrm{Hop}})=0, \tag{C1}$$

and

$$\hat{\mathbf{n}}\cdot(\mathbf{\Gamma}-\mathbf{R}-\alpha_2\hat{\mathbf{p}}_{\mathrm{Exch}})=0. \tag{C2}$$

Equations (38) and (39) can then be multiplied by real numbers γ_1 and γ_2 and added to get

$$\hat{\mathbf{n}}\cdot\left(\mathbf{\Gamma}-\mathbf{R}-\frac{\gamma_1}{\gamma_1+\gamma_2}\alpha_1\hat{\mathbf{p}}_{\mathrm{Hop}}-\frac{\gamma_2}{\gamma_1+\gamma_2}\alpha^2\hat{\mathbf{p}}_{\mathbf{Exch}}\right)=0, \tag{C3}$$

Replacing the two parameters by a single parameter $\gamma=\gamma_2/(\gamma_1+\gamma_2)$, this equation becomes

$$\hat{\mathbf{n}}\cdot(\mathbf{\Gamma}-(\mathbf{R}+\alpha_1\hat{\mathbf{p}}_{\mathbf{Hop}}+\gamma(\alpha_2\hat{\mathbf{p}}_{\mathbf{Exch}}-\alpha_1\hat{\mathbf{p}}_{\mathbf{Hop}})))=0. \tag{C4}$$

This equation shows that the intercept of the two sets above is a one-dimensional line going through the two interception points $\alpha_1\hat{\mathbf{p}}_{\mathbf{Hop}}$ and $\alpha_2\hat{\mathbf{p}}_{\mathbf{Exch}}$. Therefore the two-dimensional representation of the planes in the plane progression is given by the set of lines shown in Fig. 13.

[1] E. Wigner, Trans. Faraday Soc. **34**, 29 (1938).
[2] H. Eyring, J. Chem. Phys. **3**, 107 (1935).
[3] G. H. Vineyard, J. Phys. Chem. Solids **3**, 121 (1957).
[4] J. C. Keck, J. Chem. Phys. **32**, 1035 (1960).
[5] D. G. Truhlar, B. C. Garrett, and S. J. Klippenstein, J. Phys. Chem. **100**, 31 (1996).
[6] D. E. Makarov and H. Metiu, J. Chem. Phys. **107**, 7787 (1997).
[7] D. Chandler, J. Chem. Phys. **68**, 2959 (1978).
[8] E. A. Carter, G. Ciccotti, J. T. Hynes, and R. Kapral, Chem. Phys. Lett. **156**, 472 (1989); G. Ciccotti, M. Ferrario, D. Laria, and R. Kapral, *Simulation of Classical and Quantum Activated Processes in the Condensed Phase*, in *Progress in Computational Physics of Matter: Methods, Software, and Applications*, edited by L. Reatto and F. Manghi (World Scientific, Singapore, 1995), p. 150; M. Sprik and G. Ciccotti, J. Chem. Phys. **109**, 7737 (1998).
[9] G. K. Schenter, G. Mills, and H. Jónsson, J. Chem. Phys. **101**, 8964 (1994); G. Mills, H. Jónsson, and G. K. Schenter, Surf. Sci. **324**, 305 (1995).
[10] E. Neria, S. Fischer, and M. Karplus, J. Chem. Phys. **105**, 1902 (1996).
[11] G. Henkelman and H. Jónsson, J. Chem. Phys. **115**, 9657 (2001), following paper.
[12] G. Mills, G. K. Schenter, D. Makarov, and H. Jónsson, Chem. Phys. Lett. **278**, 91 (1997); G. Mills, G. K. Schenter, D. Makarov, and H. Jónsson, in *Classical and Quantum Dynamics in Condensed Phase Simulations*, edited by B. J. Berne, G. Ciccotti, and D. F. Coker (World Scientific, Singapore, 1998).
[13] H. Jónsson, G. Mills, and K. W. Jacobsen, in *Classical and Quantum Dynamics in Condensed Phase Simulations*, edited by B. J. Berne, G. Ciccotti, and D. F. Coker (World Scientific, Singapore, 1998).
[14] G. Henkelman and H. Jónsson, J. Chem. Phys. **113**, 9978 (2000).
[15] G. Henkelman, B. P. Uberuaga, and H. Jónsson, J. Chem. Phys. **113**, 9901 (2000).
[16] H. C. Andersen, J. Chem. Phys. **72**, 2384 (1980).
[17] A. F. Voter, Phys. Rev. Lett. **78**, 3908 (1997).
[18] M. M. Steiner, P. A. Genilloud, and J. W. Wilkins, Phys. Rev. B **57**, 10236 (1998).
[19] G. Henkelman (personal communication).
[20] D. Makarov (personal communication).
[21] P. J. Feibelman, Phys. Rev. Lett. **65**, 729 (1990).
[22] S. P. Chen and A. F. Voter, Surf. Sci. **244**, L107 (1991).
[23] J. C. Polanyi and W. H. Wong, J. Chem. Phys. **51**, 1439 (1969).